Behaviour and design of eccentrically loaded hot-rolled steel SHS and RHS stub columns at elevated temperatures

Xiang Yun[a,*], Nadiah Saari[b], Leroy Gardner[a]

[a] Department of Civil and Environmental Engineering, Imperial College London, London, UK

[b] Faculty of Civil Engineering, Universiti Teknologi MARA Johor, Pasir Gudang Campus, Masai, Johor, Malaysia

[*]Corresponding author. E-mail address: x.yun14@imperial.ac.uk

Abstract

The structural fire response of hot-rolled steel square and rectangular hollow sections (SHS and RHS) under combined compression and bending is investigated in this study through finite element (FE) modelling. The developed FE models were firstly validated against available test results on hot-rolled steel SHS/RHS subjected to combined compression and bending at elevated temperatures. Upon validation, an extensive parametric study was then carried out to examine the resistance of hot-rolled steel SHS/RHS under combined loading at elevated temperatures, covering a wide range of cross-section slendernesses, cross-section aspect ratios, combinations of loading and temperatures up to 800 °C. The numerical data, together with the experimental results, were compared with the strength predictions according to the current structural fire design rules in the European Standard EN 1993-1-2 (2002) and American Specification AISC 360-16 (2016) for hot-rolled steel SHS/RHS under combined loading. The comparisons generally indicated significant disparities in the prediction of resistance of hot-rolled steel SHS/RHS under combined loading at elevated temperatures, owing principally to inaccurate predictions of the end points of the design interaction curves. The deformation-based continuous strength method (CSM) has been shown to provide accurate strength predictions for these end points i.e. the resistances of hot-rolled steel SHS/RHS stub columns and beams at elevated temperatures. In this study, proposals are presented to extend the scope of the CSM

to the structural fire design of hot-rolled steel SHS/RHS under combined compression and bending. The CSM proposals are shown to offer improved accuracy and reliability over current design methods and are therefore recommended for incorporation into future revisions of international structural fire design codes.

Keywords: Continuous strength method; Combined loading; Elevated temperatures; Finite element modelling; Fire; Hot-rolled steel; Structural fire design

1. Introduction

The material properties of hot-rolled carbon steel at elevated temperatures are significant different from those at ambient temperature. At ambient temperature, hot-rolled carbon steel exhibits an elastic response, with a clearly defined yield point, followed by a pronounced yield plateau and a moderate degree of strain hardening [1]. At elevated temperatures, the stress-strain curve of hot-rolled carbon steel becomes distinctly nonlinear with a pronounced degradation of both strength and stiffness [2,3]. In addition to the deterioration of mechanical properties, thermal creep also accelerates at temperatures above approximately 400 °C and may affect the steel structural response [4]. A number of constitutive models have been developed to describe the nonlinear stress-strain response of hot-rolled carbon steel at elevated temperatures [5-7]. EN 1993-1-2 (2005) [5] adopts a three-stage material model as shown in Fig. 1. The first stage represents the linear portion of the stress-strain curve, where stress is directly proportional to strain up to the strain at the proportional limit $\varepsilon_{p,\theta}$ and the corresponding proportional limit stress $f_{p,\theta}$. This is followed by a nonlinear stress-strain relationship in the second stage which assumes an elliptical transition from the proportional limit stress $f_{p,\theta}$ to the stress at 2% total strain $f_{2.0,\theta}$. Finally, the third stage comprises a flat plateau up to the limiting strain $\varepsilon_{t,\theta}$ which is equal to 0.15. For temperatures below 400 °C, strain hardening beyond 2%

strain can be considered using an alternative stress-strain relationship described in Annex A of EN 1993-1-2 (2005) [5]. The Eurocode constitutive model implicitly accounts for the effect of high-temperature creep [8] and has been shown to facilitate a realistic resistance predictions for structural steel beams at elevated temperatures [4]. Morovat et al. [9] explicitly investigated the effect of creep on the buckling behaviour and strength of steel columns at elevated temperatures by using different material creep models; the study concluded that different creep models can lead to rather different column buckling resistances and that there is a clear need for more extensive and reliable creep data for carbon steels. Based upon a large dataset of elevated temperature coupon test results collected from literature, Khorasani et al. [10] found that the strength and stiffness reduction factors for hot-rolled carbon steel given in EN 1993-1-2 [5] are generally accurate, though slightly conservative, compared to those obtained from the tests. However, the deterioration of mechanical properties for high strength steels at elevated temperatures has been found to be different from that of normal strength steels, thus revised strength and stiffness reduction factors have been proposed in [11,12].

Extensive experimental and numerical research has been carried out into the fire behaviour and resistance of steel structural components, including stub columns [13-16], columns [17-23], beams [24-26] and beam columns [27-30]. However, the fire performance of hot-rolled steel square and rectangular hollow sections (SHS and RHS) under combined compression and bending has received relatively little attention. Pauli et al. [31] performed a series of cross-section tests on hot-rolled steel SHS and RHS at ambient and elevated temperatures under concentric and eccentric axial compression. The elevated temperature tests were carried out under steady state conditions at 400, 550 and 700 °C in an electrical furnace. Knobloch et al. [32] developed numerical models of hot-rolled steel sections in fire and observed that the existing codified method in EN 1993-1-2 [5] led to capacity predictions on the unsafe side for

hot-rolled steel RHS stub columns at 400 and 550 °C, where the stress-strain curves display a pronounced rounded shape. Existing provisions for structural fire design [5,33] generally utilise the traditional concept of cross-section classification and the effective width method in line with the corresponding steel design rules at room temperature, without considering the distinctive nonlinear stress-strain characteristics of carbon steel at elevated temperatures. Consequently, steel cross-sections at elevated temperatures are artificially separated into discrete behavioural classes; this approach does not, however, reflect the inherent continuous relationship between the cross-section resistance and its local slenderness. Moreover, the utilization of two different design yield strengths in EN 1993-1-2 [5] (i.e. the stress at 2% total strain $f_{2.0,\theta}$ at temperature θ for hot-rolled Class 1-3 cross-sections and the 0.2% proof stress $f_{0.2,\theta}$ at temperature θ for hot-rolled Class 4 cross-sections) results in further discontinuities in the predicted resistances at the boundary between slender (i.e. Class 4) and non-slender (Class 1-3) cross-sections. It is therefore considered necessary to develop a more consistent and accurate method for the design of hot-rolled steel cross-sections at elevated temperatures.

The continuous strength method (CSM) is a deformation-based approach that provides an alternative treatment to the concept of cross-section classification, enables a more accurate allowance to be made for the spread of plasticity and allows material strain hardening to be considered in a systematic manner. The CSM has recently been established for the design of hot-rolled and cold-formed steel structural elements and systems at room temperature [34-40], as well as the fire design of hot-rolled steel cross-sections under isolated loading (i.e. pure compression and pure bending) [41]. The present study is focused on the assessment of existing codified approaches [5,33] and the extension of the CSM to the design of hot-rolled steel SHS and RHS under combined compression and bending at elevated temperatures; assessment of the proposed method is carried out based on existing experimental results from literature [31]

and extensive numerical results conducted herein. Development and validation of the finite element (FE) models against available test results on concentrically and eccentrically loaded hot-rolled steel SHS/RHS stub columns at room temperature and under elevated temperature conditions [31] is first presented. The validated FE models are then utilised in an extensive parametric study on the resistance of hot-rolled steel SHS and RHS under combined loading at elevated temperatures, covering a wide range of cross-section slendernesses, cross-section aspect ratios, combinations of loading and elevated temperatures. Both the experimental and numerical results are used to appraise the accuracy of existing fire design provisions, including those given in the European code EN 1993-1-2 [5] and the American Standard AISC 360-16 [33], as well as to underpin the new CSM proposals for hot-rolled steel SHS and RHS under combined loading. Finally, reliability analyses are presented to assess the reliability levels of the codified and proposed design rules.

2. Summary of previous experimentation

An experimental study into the cross-sectional resistance of concentrically and eccentrically loaded hot-rolled steel SHS and RHS stub columns in fire was conducted by Pauli et al. [31]. These tests are summarized in this section and are used for the validation of the FE models as well as the appraisal of design rules in Sections 3-5 of the present paper. The measured cross-section dimensions, elevated temperature material properties and ultimate resistances of the test specimens are summarized in Table 1, where B and H are the width and height of the cross-section, t is the thickness of the cross-section, L is length of the test specimen, $E_{a,\theta}$, $f_{y,\theta}$ and $f_{u,\theta}$ are the Young's modulus, the stress at 2% total strain and the ultimate tensile strength at temperature θ, respectively, and $N_{u,test}$ is the experimental ultimate resistance, which is taken as maximum load that the specimen endured at temperature θ. In Table 1, the test specimens are labelled according to their cross-sectional shape, cross-section height, testing temperature,

bending axis and loading eccentricity. For example, the label RHS120_400C_z10 defines an RHS stub column with a nominal cross-sectional height of 120 mm, tested at an elevated temperature of 400 °C and with a nominal loading eccentricity of 10 mm to the z-axis (i.e. the weak axis). The labels without information on loading eccentricity indicate that the specimens were concentrically loaded with fixed-fixed end conditions. Note that four of the fourteen specimens were tested at ambient temperature for comparison purposes.

A three-dimensional video extensometer was employed to measure the distribution of local geometric imperfections in each test specimen. A random pattern of gypsum speckles, which served as a set of reference points, was first applied to each surface of the specimens; then a two-camera Vic-3D system was used to capture the profile of the surfaces. For each specimen, the local geometric imperfection amplitude e_0 was defined as the maximum measured absolute imperfection value for all faces, as provided in Table 1. Further details of the measurements of the local geometrical imperfections for each stub column test specimen can be found in [31].

All test specimens were made from Grade S355 structural steel. Deformation-controlled steady state tensile coupon tests were conducted to determine the material properties of the investigated cross-sections at elevated temperatures. The tensile coupons were cut in the longitudinal direction from the flat faces of the SHS and RHS used for the associated cross-sectional fire tests. The coupon tests were carried out using an electric furnace with three vertically distributed heating zones, as shown in Fig.2. The vertical elongation of the tensile coupon was measured using an extensometer consisting of two ceramic bars spaced apart by a distance of 15 mm (see Fig. 2). In the steady state tests, the coupons were firstly heated up to a target temperature; during the heating process, a small constant tensile load of approximately 300 N was applied to the coupon while the thermal elongation of the coupon was not restrained.

After reaching the target temperature, the temperature was held constant while a tensile load was applied to the coupon at a constant strain rate. Since the strain rate can have a significant influence on material properties at elevated temperatures [6], the material properties given in Table 1 are those measured at a strain rate matching that of the corresponding cross-sectional fire tests. As expected, a distinctly nonlinear stress-strain response with no sharply defined yield point was observed for the structural steel at elevated temperatures. Details of the coupon test setup and results can be found in [31].

A total of 10 steady state fire tests on hot-rolled steel SHS and RHS stub columns under concentric and eccentric axial compression were carried out using the test setup shown in Fig. 3. End plates of steel grade S355 were welded to both ends of each test specimen. The concentrically-loaded stub columns were tested with the fixed-end conditions, while for the eccentrically-loaded stub columns, two round prismatic rocker bearings were used at the top and the bottom of the specimens to achieve pinned-pinned end restraints. Adopting the steady state testing procedure, each specimen was firstly placed in an electrical furnace and then uniformly heated up to a predefined target temperature. Three thermocouples were attached to one surface of each test specimen to monitor the temperature distribution along the specimen length. After reaching steady state conditions, the test specimen was loaded under displacement control up to and beyond its peak load, with a constant strain rate of 0.1%/min. The applied vertical load and the relative vertical displacement of the test specimens were measured and recorded during the entire loading phase. Two sets of stainless steel bars were attached on both sides of the 80 mm-thick parallel end-plates (see Fig. 3(b)) and connected to two LVDTs placed underneath the furnace to measure the relative vertical displacement (i.e. end shortening) of the test specimens. The detailed test results are given in [31].

3. Numerical investigation

Numerical modelling of hot-rolled steel SHS and RHS stub columns, loaded concentrically and eccentrically at elevated temperatures, using the finite element (FE) analysis software package ABAQUS version 6.16 [42], is presented in this section. The FE models were validated using the experimental results of Pauli et al. [31] summarized in the previous section and were subsequently employed in an extensive parametric study to obtain additional data covering a wide range of cross-section sizes, cross-section slendernesses, loading combinations and elevated temperatures. The FE models used for the present numerical investigation are similar to those developed in [37-43] for stub columns and in [43,44] for cross-sections under combined compression and bending, except that the material properties at elevated temperatures were adopted herein. A detailed description of the FE models and their validation against cross-sectional tests at room temperature were presented in [37,43,44]; thus, only the key numerical modelling aspects are reported in this section.

3.1. Modelling assumptions

The four-noded doubly curved shell element with reduced integration referred to as S4R in the Abaqus element library [42] was adopted to model the hot-rolled steel SHS and RHS specimens. An element mesh size equal to one twentieth of the cross-section height H was used to discretise the flat regions of the modelled specimens, while a finer mesh of four elements was selected in the corner portions to ensure that the curved geometry could be accurately captured. As required in Abaqus [42] for the adopted element type, the engineering stress-strain curves measured in the steady state tensile coupon tests [31] were converted into the true stress and logarithmic plastic true strain curves before being incorporated into Abaqus. The boundary conditions of the test specimens were carefully simulated according to the corresponding test setup. For the FE models of the concentrically loaded stub columns, all six degrees of freedom

of the nodes at each end section were coupled to a concentric reference point. The fixed-end boundary conditions were then mimicked by restraining all degrees of freedom of the two reference points except for the longitudinal translation at the loaded end. As for the FE models of the eccentrically loaded stub columns, each end section was coupled to an eccentric reference point located at an eccentricity equal to that employed in the corresponding test. Pinned-pinned boundary conditions were then modelled by restraining appropriate degrees of freedom at the two reference points, allowing longitudinal translation at the loaded end and rotation about the axis of bending at both ends. Moreover, the eccentric reference points in the FE models were offset longitudinally from each end section by a distance equal to the distance between the specimen end section and the central axis of the rocker bearing in their corresponding tests, with the purpose of accurately simulating the effective length of the test specimens.

The lowest eigenmode-affine imperfection shapes obtained by conducting a prior Linear Buckling Analysis (LBA) of the modelled specimens under pure axial compression that feature an odd number of buckling-waves in the longitudinal direction, were applied to the FE models. The employed imperfection shapes are similar to the failure modes observed in the stub column tests [37,47]. The sensitivity of the FE simulations to varying imperfection amplitudes was apprised by comparing the resistances obtained from the models with four different imperfection amplitudes: the maximum measured amplitude for each of the test specimens and three fractions of the flat width of cross-section height h (h/400, h/300 and h/200). Residual stresses were not included in the FE models because (1) their magnitude is very low in hot-rolled tubular sections at room temperature [45,46] and (2) their magnitude is further eroded under fire conditions [18] and their influence on the local buckling of cross-sections in fire has been shown to be negligible [18,48]. The loading procedure employed in the FE analyses

mirrored that used in the tests, whereby a predefined temperature field using the Abaqus keywords *TEMPERATURE [42] was firstly applied to the FE models, leading to the development of thermal strains and the modification of the material stress-strain response; an axial load was then imposed by specifying an axial displacement to the reference point at the loaded end of the stub columns. The modified Riks method [42] was used to perform the FE analyses, enabling the full load-deformation histories, including the post-ultimate paths, to be captured.

3.2. Validation

Validation of the FE models was achieved by comparing the ultimate loads, load-end shortening curves and failure modes obtained from the numerical simulations with those obtained from the experiments presented in [31] and summarised in Section 2. The ratios of the ultimate loads obtained from the tests $N_{u,test}$ to those derived from the FE models $N_{u,FE}$ with the four different imperfection amplitudes are given in Table 2. The comparisons indicate that the amplitude of local geometric imperfection has only a minor influence on the ultimate resistances of the investigated hot-rolled steel SHS and RHS, which fall into the non-slender range (i.e. Class 1-3) according to EN 1993-1-2 [5]. The FE models with the local imperfection amplitude of $h/200$ were found to provide the closest ultimate resistances to those obtained from the FE models with the measured imperfection amplitudes. Moreover, using the local imperfection amplitude of $h/200$ in the FE models, which is consistent with the recommendations in EN 1993-1-5 [49], also provides reasonably accurate yet safe-sided predictions of the test ultimate loads, with the mean value of the ratio of $N_{u,test}/N_{u,FE}$ being 1.07 and the corresponding coefficient of variation being 0.073. Thus, the amplitude of $h/200$ was adopted in the parametric studies described in the following subsection. The relatively large deviation between the test and numerical results for the RHS120_550C_z10 specimen is

unexpected, but may relate to the greater uncertainties associated with structural fire tests compared to those at room temperature, the sensitivity to loading rate, variations of temperature within the furnace and departure from the intended loading eccentricities. The experimentally obtained load-end shortening curves and failure modes were also compared with their numerical counterparts, as displayed for typical examples in Figs. 4 and 5, where good agreement can be observed. The generally conservative FE predictions, as shown in Fig.4, may also be due to the mentioned uncertainties and variations in performing the stub column tests at elevated temperatures. Overall, the FE models have been shown to be capable of accurately replicating the cross-sectional tests at both ambient and elevated temperatures, and are thus deemed suitable for performing numerical parametric studies.

3.3. Parametric studies

Considering various cross-section slendernesses, cross-section aspect ratios, combinations of loading and elevated temperature levels, numerical parametric studies were conducted, using the validated FE models described in Section 3.2, to investigate the resistances of hot-rolled steel SHS and RHS under combined compression and bending at elevated temperatures. The modelled specimens covered all four cross-section classes at elevated temperatures according to the slenderness limits of Eurocode 3 [5,50], but remained within the range of non-slender sections at elevated temperature θ with elevated temperature cross-section slenderness $\overline{\lambda}_{p,\theta}$ being less than or equal to 0.68 [41]. The elevated temperature slenderness $\overline{\lambda}_{p,\theta}$ is defined as the square root of the ratio of the yield strength at temperature θ, which is taken herein as the 0.2% proof stress $f_{0.2,\theta}$ at temperature θ, to the elastic local buckling stress $f_{cr,\theta}$ of the cross-section under the applied loading conditions at temperature θ. The elastic local buckling stress of the full cross-section $f_{cr,\theta}$ was determined by using the finite strip software CUFSM [51] in

the present study to account for element interaction, as given in Table 1; similar results were obtained using the formulae presented in [52].

Three different cross-section aspect ratios (H/B = 1.00, 1.33 and 2.00) were considered in the parametric studies; the outer height H was kept constant at 200 mm while three different outer widths of 200, 150 and 100 mm were adopted. A wide range of cross-section slendernesses was achieved by varying the cross-section thickness from 5 mm to 16 mm in intervals of 1 mm. For each modelled cross-section, a combination of 10 different loading eccentricities e, which were varied from 10 mm to 500 mm, and five different loading angles α (0°, 30°, 45°, 60° and 90°) was considered to provide a broad range of loading combinations. The definitions of the loading eccentricity e and loading angle α are illustrated in Fig. 6. Note that loading angles of 0° and 90° corresponding to major and minor axis bending plus compression, respectively, while the intermediate angles (30°, 45° and 60°) represent biaxial bending plus compression. The specimen length was set equal to three times the average outer cross-section dimension (i.e. $(H+B)/2$) in all models, while the internal corner radius r_i was set equal to the cross-section thickness t.

The stress-strain relationship for hot-rolled Grade S355 steel at elevated temperatures, as defined in EN 1993-1-2 [5] (see Fig. 1), was adopted in the parametric studies. Six different elevated temperatures ranging from 300 °C to 800 °C in intervals of 100 °C were investigated for each modelled specimen. Note that for 300 °C, the alternative stress-strain curve given in Annex A of EN 1993-1-2 [5], which allows for strain hardening for temperatures below 400 °C, was adopted. The behaviour and design of hot-rolled steel SHS and RHS under combined loading at room temperature was investigated by Yun et al [44], and is thus not covered in the present study. In total, over 5000 numerical parametric results were generated, which are

employed, together with the test results, to assess existing design approaches and new CSM proposals for determining resistances of hot-rolled steel SHS and RHS under combined compression and bending at elevated temperatures.

4. Discussion and assessment of design rules

In this section, three methods for the fire design of hot-rolled steel SHS and RHS under combined compression and bending, including two existing design approaches set out in EN 1993-1-2 [5] and AISC 360-16 [33], and a new design proposal based on the CSM, are described and assessed. The accuracy of these design methods is evaluated by comparing the test [31] and FE ultimate loads $N_{u,test/FE}$ with those predicted based on the design rules $N_{u,pred}$. A value of $N_{u,test/FE}/N_{u,pred}$ greater than unity indicates a safe-sided resistance prediction. Note that the calculations were based on the measured (or modelled) material properties, and all resistance factors (i.e. partial safety factors) were set to equal to unity. As specified in the code, for the EN 1993-1-2 [5] resistance calculations, the elevated temperature strength at 2% total strain $f_{2.0,\theta}$ was used as the effective yield strength for structural members with non-slender (Class 1, 2 and 3) cross-sections, while the elevated temperature 0.2% proof strength was used for members with slender (Class 4) cross-sections. The same principle was also employed when calculating the design strengths according to AISC 360-16 [33].

4.1. European code EN 1993-1-2 (EC3)

The design expressions in EN 1993-1-2 [5] for hot-rolled steel cross-sections subjected to combined bending and axial compression in fire follow the same format as the room temperature beam-column member design equations in EN 1993-1-1 [50]. There are no specific resistance expressions for cross-section design; instead, cross-section design is treated as a special case of member design. Since short SHS and RHS members are not susceptible to

lateral torsional buckling, only in-plane bending/buckling is considered herein. The codified design formula for hot-rolled steel SHS and RHS under combined loading at elevated temperatures is given by Eq. (1), where $N_{\mathrm{fi,Ed}}$ is the design axial load for the fire design situation, $M_{\mathrm{y,fi,Ed}}$ and $M_{\mathrm{z,fi,Ed}}$ are the design maximum first order bending moments about the major and minor axes, respectively, $(N_{\mathrm{b,fi,Rd}})_{\min}$ is equal to a lower value of the flexural buckling resistances about the major ($N_{\mathrm{b,y,fi,Rd}}$) and minor ($N_{\mathrm{b,z,fi,Rd}}$) axes for the fire design situation, $M_{\mathrm{Rd,y}}$ and $M_{\mathrm{Rd,z}}$ are the design bending resistances about the major and minor axes at ambient temperature, respectively, $k_{\mathrm{y},\theta}$ is the reduction factor for the yield strength at temperature θ, which is equal to the ratio of the effective yield strength at temperature θ (i.e. $f_{2.0,\theta}$ for Class 1-3 sections and $f_{0.2,\theta}$ for Class 4 sections) to the steel yield strength at ambient temperature f_{y}, and k_{y} and k_{z} are interaction factors, calculated from Eqs. (2) and (3), respectively.

$$\frac{N_{\mathrm{fi,Ed}}}{(N_{\mathrm{b,fi,Rd}})_{\min}}+\frac{k_{\mathrm{y}}M_{\mathrm{y,fi,Ed}}}{k_{\mathrm{y},\theta}M_{\mathrm{Rd,y}}}+\frac{k_{\mathrm{z}}M_{\mathrm{z,fi,Ed}}}{k_{\mathrm{y},\theta}M_{\mathrm{Rd,z}}}\le 1 \tag{1}$$

$$k_{y}=1-\frac{\mu_{\mathrm{y}}N_{\mathrm{fi,Ed}}}{N_{\mathrm{b,y,fi,Rd}}}\le 3,\ \text{with}\ \mu_{\mathrm{y}}=\left(2\beta_{\mathrm{M,y}}-5\right)\bar{\lambda}_{\mathrm{y},\theta}+0.44\beta_{\mathrm{M,y}}+0.29\le 0.8 \tag{2}$$

$$k_{\mathrm{z}}=1-\frac{\mu_{\mathrm{z}}N_{\mathrm{fi,Ed}}}{N_{\mathrm{b,z,fi,Rd}}}\le 3,\ \text{with}\ \mu_{\mathrm{z}}=\left(1.2\beta_{\mathrm{M,z}}-3\right)\bar{\lambda}_{\mathrm{z},\theta}+0.71\beta_{\mathrm{M,z}}-0.29\le 0.8 \tag{3}$$

In Eqs. (2) and (3), $\beta_{\mathrm{M,y}}$ and $\beta_{\mathrm{M,z}}$ are equivalent uniform moment factors determined from Fig. 4.2 of EN 1993-1-2 [5]. For eccentrically loaded stub columns subjected to uniform first-order bending moment, which are the focus of the present study, $\beta_{\mathrm{M,y}}$ and $\beta_{\mathrm{M,z}}$ are both equal to 1.1. The design rules in EN 1993-1-2 [5] for determining the flexural buckling resistances of columns in fire conditions $N_{\mathrm{b,fi,Rd}}$ are generally the same as those in EN 1993-1-1 [50], adopting

the traditional Perry-Robertson concept. The design formulae for determining $N_{b,fi,Rd}$ are given by Eqs. (4) and (5),

$$N_{b,fi,Rd} = \chi_{fi} A k_{y,\theta} f_y \text{ for Class 1-3 sections} \quad (4)$$

$$N_{b,fi,Rd} = \chi_{fi} A_{eff} k_{y,\theta} f_y \text{ for Class 4 sections} \quad (5)$$

where A is the cross-sectional area for Class 1-3 sections, A_{eff} is the effective cross-sectional area for Class 4 sections calculated using the effective width method, following the provisions of EN 1993-1-1 [50] and EN 1993-1-5 [49], and χ_{fi} is the reduction factor for flexural buckling in the fire design situation calculated as

$$\chi_{fi} = \frac{1}{\varphi_\theta + \sqrt{\varphi_\theta^2 - \bar{\lambda}_\theta^2}} \text{ with } \varphi_\theta = 0.5\left(1 + \alpha\bar{\lambda}_\theta + \bar{\lambda}_\theta^2\right) \text{ and } \alpha = 0.65\sqrt{235/f_y} \quad (6)$$

in which $\bar{\lambda}_\theta$ is the non-dimensional slenderness at temperature θ defined by Eq. (7).

$$\bar{\lambda}_\theta = \bar{\lambda}\sqrt{\frac{k_{y,\theta}}{k_{E,\theta}}} \quad (7)$$

In Eq. (7), $\bar{\lambda}$ is the non-dimensional slenderness at room temperature and $k_{E,\theta}$ is the reduction factor for Young's modulus at temperature θ. Note that the cross-section classification at elevated temperatures is determined based on the same rules as for ambient temperature design [50], but with a reduced value for the material factor ε of $0.85\sqrt{235/f_y}$. For the ambient

temperature cross-section bending resistance M_{Rd}, EN 1993-1-1 [50] prescribes the use of the plastic moment capacity $M_{pl,Rd}$, the elastic moment capacity $M_{el,Rd}$ and a reduced effective moment capacity $M_{eff,Rd}$ for Class 1 or 2, Class 3 and Class 4 sections, respectively.

The ratios of the test (or FE) ultimate loads to the EC3 predicted resistances $N_{u,test/FE}/N_{u,EC3}$ are plotted against the cross-section slendernesses $\overline{\lambda}_{p,\theta}$ at elevated temperature θ, determined from the CUFSM [51], in Fig. 7 for uniaxial bending plus compression and Fig. 8 for biaxial bending plus compression. A quantitative evaluation of the EC3 and other design approaches is presented in Table 3. It can be seen from Figs 7 and 8 that EC3 yields somewhat scattered resistance predictions for Class 1 and 2 sections, with a general transition from under-predictions to over-predictions with increasing $\overline{\lambda}_{p,\theta}$ values. For Class 3 sections, it is observed from Fig. 7 that the EC3 resistance predictions are generally on the unsafe side for specimens under uniaxial bending plus compression, with the mean value of $N_{u,test/FE}/N_{u,EC3}$ being 0.85 and the corresponding COV equal to 0.092 as indicated in Table 3. For Class 3 sections subjected to biaxial bending plus compression, EC3 provides accurate resistance predictions on average with the mean value of $N_{u,test/FE}/N_{u,EC3}$ equal to 1.05, but with many predictions on the unsafe side thus leading to a relatively high COV of 0.154, as shown in Fig. 8 and Table 3. The EC3 over-predictions of resistance for Class 3 sections may result from the fact that local buckling occurs prior to the attainment of the effective yield strength at elevated temperatures $f_{y,\theta}$, which is defined as the strength at 2% total strain $f_{2.0,\theta}$. Conversely, use of the 0.2% proof strength $f_{0.2,\theta}$ as the design yield strength when calculating the resistance of Class 4 cross-sections can be seen to result in conservative predictions. As reported in Table 3, the mean ratios of $N_{u,test/FE}/N_{u,EC3}$ are 1.37 and 1.56, with the corresponding COV values equal to 0.107 and 0.116, for SHS/RHS with Class 4 cross-sections subjected to compression plus uniaxial bending and biaxial bending, respectively. Owing to the discrete nature of the cross-section

classification system and the specification of two distinct levels of design yield strength for Class 1-3 and Class 4 sections, EC3 also has discontinuous steps in the resistance predictions at the boundaries between the different classes, which does not reflect the observed structural response. Overall, EC3 yields resistance predictions that are, in some instances, highly conservative and, in others, on the unsafe side. The codified design rules can be improved through the adoption of more accurate cross-section resistances under pure compression and pure bending (serving as the end points of the interaction curves) by using more advanced design methods, and the development of a revised shape for the interaction curves, anchored to these new end points.

4.2. American specification AISC 360-16 (AISC)

The design rules provided in AISC 360-16 [33] for determining cross-sectional strengths at elevated temperatures are the same as those at ambient temperature, except for the use of the material strengths and stiffnesses at elevated temperatures. The AISC design equations for doubly symmetric cross-sections subjected to combined bending and compression in fire satiations are given by Eqs. (8) and (9), where $N_{c.fi}$ is the cross-sectional resistance under pure compression for the fire design situation, $M_{c.y}$ and $M_{c.z}$ are the cross-sectional bending moment resistances about major and minor axes, respectively, and $\alpha_{m.y}$ and $\alpha_{m.z}$ are the magnification factors employed to account for second order effects, though these are insignificant for the short specimens examined herein. For either principal axis, α_m is equal to $1/(1\text{-}N_{fi,Ed}/N_{cr,fi})$, where $N_{cr,fi}$ is the Euler buckling load of the column at elevated temperatures.

$$\frac{N_{\mathrm{fi,Ed}}}{N_{\mathrm{c,fi}}}+\frac{8}{9}\left(\frac{\alpha_{\mathrm{m,y}}M_{\mathrm{y,fi,Ed}}}{k_{\mathrm{y},\theta}M_{\mathrm{c,y}}}+\frac{\alpha_{\mathrm{m,z}}M_{\mathrm{z,fi,Ed}}}{k_{\mathrm{y},\theta}M_{\mathrm{c,z}}}\right)\leq 1,\ \text{for}\ \frac{N_{\mathrm{fi,Ed}}}{N_{\mathrm{c,fi}}}\geq 0.2 \tag{8}$$

$$\frac{N_{\mathrm{fi,Ed}}}{2N_{\mathrm{c,fi}}}+\frac{\alpha_{\mathrm{m,y}}M_{\mathrm{y,fi,Ed}}}{k_{\mathrm{y},\theta}M_{\mathrm{c,y}}}+\frac{\alpha_{\mathrm{m,z}}M_{\mathrm{z,fi,Ed}}}{k_{\mathrm{y},\theta}M_{\mathrm{c,z}}}\le 1,\ \text{for}\ \frac{N_{\mathrm{fi,Ed}}}{N_{\mathrm{c,fi}}}<0.2 \tag{9}$$

According to the AISC Specification, the compressive strength of members at elevated temperatures $N_{\mathrm{c.fi}}$ is determined from Eqs. (10) and (11), where $f_{\mathrm{e},\theta}$ is the minor axis elastic buckling stress at elevated temperature θ. The resistance of stub columns in fire calculated using EC3 ($N_{\mathrm{b,fi,Rd}}$) and the AISC Specification ($N_{\mathrm{c.fi}}$) are similar for non-slender cross-sections (Class 1-3 sections) since the parameters employed in their design expressions to account for member second-order effects are both approximately equal to unity. However, the strength predictions for stub columns with slender cross-sections (Class 4 sections) can be rather different due to their adoption of different cross-section slenderness limits and effective width equations. For the resistance of cross-sections in bending, the AISC Specification adopts the plastic moment capacity $M_{\mathrm{pl,Rd}}$ for compact sections (equivalent to Class 1 and 2 sections in EC3), which is the same as prescribed in EC3 for Class 1 and 2 sections, and considers partial plasticity for non-compact sections (equivalent to Class 3 sections in EC3), resulting in bending resistance predictions that lie between $M_{\mathrm{el,Rd}}$ and $M_{\mathrm{pl,Rd}}$. For slender cross-sections (equivalent to Class 4 sections in EC3), a lower bending moment resistance is determined using the traditional effective width method.

$$N_{\mathrm{c,fi}}=\left(0.658^{\frac{k_{\mathrm{y},\theta}f_{\mathrm{y}}}{f_{\mathrm{e},\theta}}}\right)k_{\mathrm{y},\theta}f_{\mathrm{y}}A,\ \text{for non-slender sections (Class 1-3 sections)} \tag{10}$$

$$N_{\mathrm{c,fi}}=\left(0.658^{\frac{k_{\mathrm{y},\theta}f_{\mathrm{y}}}{f_{\mathrm{e},\theta}}}\right)k_{\mathrm{y},\theta}f_{\mathrm{y}}A_{\mathrm{eff}},\ \text{for slender sections (Class 4 sections)} \tag{11}$$

A graphical assessment of the AISC design provisions was made by plotting the ratios of $N_{u,test/FE}/N_{u,AISC}$ versus $\bar{\lambda}_{p,\theta}$, as shown in Figs. 9 and 10 for hot-rolled steel SHS and RHS subjected to compression plus uniaxial and biaxial bending, respectively. Note that, as indicated in Figs. 7-10, owing to the different slenderness limits and design rules to classify cross-sections in EC3 and the AISC Specification, many cross-sections investigated in the present study that are classified as non-slender (i.e. Class 1-3) according to EC3 are classified as slender sections according to the AISC Specification. As reported in Table 3, the AISC Specification generally yields more conservative and less scattered resistance predictions than EC3 for compact sections, due mainly to the adopted interaction curves. It can be seen from Table 3 and Figs. 9 and 10 that the AISC Specification leads to improved results over EC3 for both non-compact and slender sections, but is still unduly conservative for slender sections and with a significant number of the resistance predictions for non-compact sections lying on the unsafe side.

4.3. Continuous strength method (CSM)

The shortcomings in current structural fire design rules for hot-rolled steel SHS and RHS under combined loading result largely from the discrete nature of the cross-section classification framework and from the inaccurate resistance predictions for cross-sections under pure compression and pure bending, which serve as the end points of the design interaction curves. The continuous strength method (CSM) is a deformation-based method, in which the resistances of cross-sections are related, in a continuous fashion, to their deformation capacities, abandoning the concept of cross-section classification and thus eliminating the artificial steps in resistance predictions. The CSM has recently been applied to structural fire design of cross-sections under isolated loading (i.e. pure compression and pure bending) [41], and has been shown to provide more accurate and less scattered resistance predictions than are

achieved using the current EC3 provisions. In this subsection, the CSM design procedure for cross-sections at elevated temperatures is briefly summarised, and extension of the CSM to the calculation of the resistance of SHS and RHS under combined loading at elevated temperatures is described and assessed.

The first step towards the application of the CSM to the design of steel cross-sections at elevated temperatures lies in the determination of a suitable base curve, which can provide a continuous relationship between the cross-section deformation capacity to the cross-section slenderness $\overline{\lambda}_{p,\theta}$ at temperature θ. The cross-section deformation capacity used in the CSM base curve is defined as the ratio of the maximum compressive strain $\varepsilon_{csm,\theta}$ that a cross-section can sustain prior to failure at elevated temperature θ to the yield strain $\varepsilon_{y,\theta}$ at elevated temperature θ ($\varepsilon_{y,\theta} = f_{0.2,\theta}/E_{a,\theta}$). The CSM base curve developed for stainless steel and carbon steel cross-sections at ambient temperature, as given in Eq. (12), has been found to provide a reasonable (generally lower-bound) fit to hot-rolled steel cross-sections at elevated temperatures. The base curve defined in Eq. (12) is suitable for cross-sections with $\overline{\lambda}_{p,\theta}$ less than or equal to 0.68, which is the focus of the present study. Two upper limits are set on the cross-section deformation capacity (i.e. $\varepsilon_{csm,\theta}/\varepsilon_{y,\theta}$): the first limit of 15 is to avoid excessive deformations while the second limit of $\varepsilon_{lim,\theta}/\varepsilon_{y,\theta}$ is related to the adopted CSM material model to prevent over-prediction of material strength. The limit strain $\varepsilon_{lim,\theta}$ at elevated temperature θ is taken as 0.03 if strain hardening after 2% strain is considered (for θ < 400 °C in EC3) and as 0.02 if the strain hardening after 2% strain is ignored (for θ ≥ 400 °C in EC3).

$$\frac{\varepsilon_{csm,\theta}}{\varepsilon_{y,\theta}} = \frac{0.25}{\overline{\lambda}_{p,\theta}^{3.6}} \text{ but} \leq \min\left(15, \frac{\varepsilon_{lim,\theta}}{\varepsilon_{y,\theta}}\right), \text{ for } \overline{\lambda}_{p,\theta} \leq 0.68 \quad (12)$$

Unlike in the codified fire design methods [5,33], where the design yield strength is defined as either $f_{2.0,\theta}$ or $f_{0.2,\theta}$, in the CSM, the design stress $\sigma_{csm,\theta}$ at elevated temperature θ is related to the CSM limiting strain $\varepsilon_{csm,\theta}$ of the cross-section through the CSM bilinear material model, as illustrated in Fig. 11 and given by Eq. (13). Note that, for comparison purposes, the stress-strain curves obtained from the tensile coupon tests [31] have also been plotted in Fig. 11 in a manner that allows comparison with the adopted CSM bilinear material model. The model can be seen to capture the general strain hardening behaviour of carbon steels at elevated temperatures, with the stress predictions over the strain range from $\boldsymbol{\varepsilon_{y,\theta}}$ to 2% lying on the safe side. Upon determination of $\varepsilon_{csm,\theta}$ and $\sigma_{csm,\theta}$, the CSM compression, major axis bending and minor axis bending resistances of SHS and RHS at elevated temperatures ($N_{csm,\theta}$, $M_{csm,y,\theta}$ and $M_{csm,z,\theta}$) can be calculated from Eqs. (14)-(16), respectively. In Eqs. (14)-(16), W_{el} and W_{pl} are the elastic and plastic section moduli, respectively, the suffixes 'y' and 'z' denote bending about major and minor axes, respectively, and $\gamma_{M,fi}$ is the partial factor for fire design.

$$\sigma_{csm,\theta} = f_{0.2,\theta} + E_{sh,\theta}\left(\varepsilon_{csm,\theta} - \varepsilon_{y,\theta}\right) \text{ with } E_{sh,\theta} = \frac{f_{2.0,\theta} - f_{0.2,\theta}}{0.02 - \varepsilon_{y,\theta}} \tag{13}$$

$$N_{csm,\theta} = \frac{A\sigma_{csm,\theta}}{\gamma_{M,fi}} \tag{14}$$

$$M_{csm,y,\theta} = \frac{W_{pl,y} f_{0.2,\theta}}{\gamma_{M,fi}}\left[1 + \frac{E_{sh,\theta}}{E_{a,\theta}}\frac{W_{el,y}}{W_{pl,y}}\left(\frac{\varepsilon_{csm,\theta}}{\varepsilon_{y,\theta}} - 1\right) - \left(1 - \frac{W_{el,y}}{W_{pl,y}}\right)\left(\frac{\varepsilon_{csm,\theta}}{\varepsilon_{y,\theta}}\right)^{-2}\right] \tag{15}$$

$$M_{csm,z,\theta} = \frac{W_{pl,z} f_{0.2,\theta}}{\gamma_{M,fi}}\left[1 + \frac{E_{sh,\theta}}{E_{a,\theta}}\frac{W_{el,z}}{W_{pl,z}}\left(\frac{\varepsilon_{csm,\theta}}{\varepsilon_{y,\theta}} - 1\right) - \left(1 - \frac{W_{el,z}}{W_{pl,z}}\right)\left(\frac{\varepsilon_{csm,\theta}}{\varepsilon_{y,\theta}}\right)^{-2}\right] \tag{16}$$

Extension of the CSM to the fire design of hot-rolled steel SHS and RHS under combined loading is sought by using the interaction formulae and coefficients employed in EN 1993-1-2 but with the adoption of the CSM cross-section resistances in compression ($N_{csm,\theta}$) and bending ($M_{csm,y,\theta}$ and $M_{csm,z,\theta}$) as the new end points. The proposed CSM interaction formula is given by Eq. (17), where $(\chi_{fi})_{min}$ is the taken as the lower value of the reduction factors for flexural buckling about the major and minor axis in the fire design situation, and $k_{y,csm}$ and $k_{z,csm}$ are the CSM interaction factors determined based on the CSM cross-section compression resistance, as given by Eqs. (18) and (19), respectively. Note that in the CSM proposal, the reduction factor $k_{y,\theta}$ used in Eq (7) for the calculation of the non-dimensional slenderness $\overline{\lambda}_\theta$ is taken as the ratio of $f_{0.2,\theta}/f_y$ for all investigated cross-sections. Note also that owing to the focus on cross-section behaviour (i.e. short members in the context of the present paper), the values of χ_{fi} are all very close to unity, and the range of applicability of the current proposals is $\overline{\lambda}_\theta < 0.2$.

$$\frac{N_{fi,Ed}}{(\chi_{fi})_{min} N_{csm,\theta}} + \frac{k_{y,csm} M_{y,fi,Ed}}{M_{csm,y,\theta}} + \frac{k_{z,csm} M_{z,fi,Ed}}{M_{csm,z,\theta}} \leq 1 \tag{17}$$

$$k_{y,csm} = 1 - \frac{\mu_y N_{fi,Ed}}{\chi_{y,fi} N_{csm,\theta}} \leq 3, \text{ with } \mu_y = \left(2\beta_{M,y} - 5\right)\overline{\lambda}_{y,\theta} + 0.44\beta_{M,y} + 0.29 \leq 0.8 \tag{18}$$

$$k_{z,csm} = 1 - \frac{\mu_z N_{fi,Ed}}{\chi_{z,fi} N_{csm,\theta}} \leq 3, \text{ with } \mu_z = \left(1.2\beta_{M,z} - 3\right)\overline{\lambda}_{z,\theta} + 0.71\beta_{M,z} - 0.29 \leq 0.8 \tag{19}$$

The accuracy of the proposed CSM for predicting the resistances of hot-rolled steel SHS and RHS under combined loading at elevated temperatures is assessed through comparisons against the test and FE results, following a similar approach to that used for the evaluation of EC3, as shown in Table 3 and Figs 12 and 13. The comparisons generally indicate that the CSM

provides significantly improved consistency of predictions compared to the existing design methods, with COV values of $N_{u,test/FE}/N_{u,csm}$ equal to 0.058 and 0.100 for the scenarios of compression plus uniaxial and biaxial bending, respectively, as reported in Table 3. The CSM generally yields slightly more conservative resistance predictions on average, but with a significantly reduced number of predictions on the unsafe side, indicating the improved safety of the proposed method. The conservatism in the proposed method may result from the adopted simplified CSM material model, which underestimates the steel strength over the strain range from $\varepsilon_{y,\theta}$ to 2%, as illustrated in Fig. 11, and from the employed EC3 interaction factors, which define the shape of the moment-compression (M-N) curve. This indicates that there is further scope for improving the proposed CSM by utilising an alternative material model and interaction factors. Note that when the CSM is implemented within a framework of design by advanced inelastic analysis, there is no penalty (in terms of complexity of calculations) in using a more sophisticated material model, since internal forces and moments are computed numerically [39,52-54].

5. Reliability analyses

In this section, statistical analyses are carried out to assess the reliability level of the existing and proposed fire design methods for hot-rolled steel SHS and RHS under combined loading, according to the reliability criteria set out by Kruppa [55]. Three reliability criteria were specified to compare the theoretical (predicted) resistance $r_{t,i}$, calculated using the considered design approach, with the corresponding experimental or FE resistance $r_{e,i}$. These criteria are described below and illustrated in Fig. 14.

- Criterion 1: The percentage of the theoretical (predicted) resistances $r_{t,i}$ on the unsafe side by more than 15% of the benchmark experimental or FE resistances $r_{e,i}$ (i.e. $r_{t,i} > 1.15 r_{e,i}$) should be zero.
- Criterion 2: The percentage of the theoretical (predicted) resistances $r_{t,i}$ on the unsafe side of the benchmark experimental or FE resistances $r_{e,i}$ (i.e. $r_{t,i} > r_{e,i}$) should be less than 20%.
- Criterion 3: The mean value of all percentage differences between the theoretical (predicted) resistances $r_{t,i}$ and the benchmark experimental or FE resistances $r_{e,i}$ should be less than zero.

The reliability assessment results for the three different fire design methods are summarised in Table 4. As shown in Table 4, the existing fire design methods provided in EN 1993-1-2 [5] and AISC 360-16 [33] frequently violate the criteria set out by Kruppa [55], while the CSM satisfies all three criteria, indicating that the proposed method is able to provide reliable resistance predictions for hot-rolled steel SHS and RHS under combined compression and bending at elevated temperatures with a value of $\gamma_{M,fi}$ equal to unity.

6. Calculation example

This section provides a worked example to demonstrate the calculation procedure of the CSM for the design of hot-rolled steel cross-sections under combined loading at elevated temperatures. The geometric and material properties of one tested specimen [31] have been used for the demonstration and all partial safety factors have been set equal to unity, thereby facilitating direct comparison with the test results.

The CSM predicted resistance of the RHS120_400C_z10 [31] can be determined as follows:

Cross-section dimensions and material properties:

H = 119.4 mm B = 60.6 mm t = 4.0 mm e_z = 9.4 mm A = 1320.6 mm^2 E = 210 GPa

$E_{a,\theta}$ = 160.7 GPa $f_{0.2,\theta}$ = 249 MPa $f_{2.0,\theta}$ = 365 MPa $f_{u,\theta}$ = 454 MPa f_y = 355 MPa

$\varepsilon_{y,\theta} = f_{0.2,\theta}/E_{a,\theta}$ = 0.002 $W_{el,z}$ = 27061 mm^3 $W_{pl,z}$ = 31083 mm^3 $k_{y,T} = f_{0.2,\theta}/f_y$ = 0.70

$k_{E,T} = E_{a,\theta}/E$ = 160.7/210 = 0.77 $\bar{\lambda}_z$ = 0.188 θ = 400 °C $\beta_{M,z}$ = 1.1

Step 1: Determine cross-section slenderness $\bar{\lambda}_{p,\theta}$

$f_{0.2,\theta}$ = 249 MPa, $f_{cr,\theta}$ = 792 MPa from CUFSM [51].

$$\bar{\lambda}_{p,\theta} = \sqrt{f_{0.2,\theta} / f_{cr,\theta}} = \sqrt{249/792} = 0.56 .$$

Step 2: Determine the cross-section deformation capacity

$$\frac{\varepsilon_{csm,\theta}}{\varepsilon_{y,\theta}} = \frac{0.25}{\bar{\lambda}_{p,\theta}^{3.6}} = \frac{0.25}{0.56^{3.6}} = 2.01 \left(\le \text{lesser}\left(15, \frac{\varepsilon_{lim,\theta}}{\varepsilon_{y,\theta}} = 12.91 \right) \right).$$

Step 3: Determine the CSM stress $\sigma_{csm,\theta}$

$$E_{sh,\theta} = \frac{f_{2.0,\theta} - f_{0.2,\theta}}{0.02 - \varepsilon_{y,\theta}} = 6273 \text{ MPa} ,$$

$$\sigma_{csm,\theta} = f_{0.2,\theta} + E_{sh,\theta}\left(\varepsilon_{csm,\theta} - \varepsilon_{y,\theta}\right) = 259 \text{ MPa} .$$

Step 4: Determine the CSM cross-section compression and bending resistances

$$N_{csm,\theta} = \frac{A\sigma_{csm,\theta}}{\gamma_{M,fi}} = \frac{1320.6 \times 259}{1.0} = 342 \text{ kN} ,$$

$$M_{csm,z,\theta} = \frac{W_{pl,z} f_{0.2,\theta}}{\gamma_{M,fi}} \left[1 + \frac{E_{sh,\theta}}{E_{a,\theta}} \frac{W_{el,z}}{W_{pl,z}} \left(\frac{\varepsilon_{csm,\theta}}{\varepsilon_{y,\theta}} - 1 \right) - \left(1 - \frac{W_{el,z}}{W_{pl,z}} \right) \left(\frac{\varepsilon_{csm,\theta}}{\varepsilon_{y,\theta}} \right)^{-2} \right]$$

$$= \frac{31083 \times 249}{1.0} \left[1 + \frac{6273}{160700} \times \frac{27061}{31083} \times (2.01 - 1) - \left(1 - \frac{27061}{31083} \right) \times (2.01)^{-2} \right]$$

$$= 7.76 \text{ kNm}$$

Step 5: Determine the reduction factor for flexural buckling

$\alpha = 0.65\sqrt{235/\ f_{\mathrm{y}}} = 0.65\sqrt{235/355} = 0.43,$

$\bar{\lambda}_{\theta,\mathrm{z}} = \bar{\lambda}_{\mathrm{z}}\sqrt{\frac{k_{\mathrm{y},\theta}}{k_{\mathrm{E},\theta}}} = 0.188\times\sqrt{\frac{0.70}{0.77}} = 0.179$, which is less than 0.2 and thus within the range of application of the CSM,

$\varphi_{\theta,\mathrm{z}} = 0.5\left(1+\alpha\bar{\lambda}_{\theta,\mathrm{z}}+\bar{\lambda}^{2}_{\theta,\mathrm{z}}\right) = 0.5\times\left(1+0.43\times0.179+0.179^{2}\right) = 0.55,$

$\chi_{\mathrm{z,fi}} = \frac{1}{\varphi_{\theta,\mathrm{z}}+\sqrt{\varphi_{\theta,\mathrm{z}}{}^{2}-\bar{\lambda}^{2}_{\theta,\mathrm{z}}}} = \frac{1}{0.55+\sqrt{0.55^{2}-0.179^{2}}} = 0.93.$

Step 6: Determine the CSM interaction factor

$\mu_{\mathrm{z}} = \left(1.2\beta_{\mathrm{M,z}}-3\right)\bar{\lambda}_{\mathrm{z},\theta}+0.71\beta_{\mathrm{M,z}}-0.29 = \left(1.2\times1.1-3\right)\times0.179+0.71\times1.1-0.29 = 0.19 \le 0.8$

$k_{\mathrm{z,csm}} = 1-\frac{\mu_{\mathrm{z}}N_{\mathrm{fi,Ed}}}{\chi_{\mathrm{z,fi}}N_{\mathrm{csm},\theta}} = 1-\frac{0.19N_{\mathrm{fi,Ed}}}{0.93\times342} = 1-0.0006N_{\mathrm{fi,Ed}}.$

Step 7: Determine the CSM cross-section resistance under combined loading

Substituting the $k_{\mathrm{z,csm}}$ expression and the values of $\chi_{\mathrm{z,fi}}$, $N_{\mathrm{csm},\theta}$, $k_{\mathrm{z,csm}}$ and $M_{\mathrm{csm,z},\theta}$ into the following equation,

$\frac{N_{\mathrm{fi,Ed}}}{\chi_{\mathrm{z,fi}}N_{\mathrm{csm},\theta}}+\frac{k_{\mathrm{z,csm}}M_{\mathrm{z,fi,Ed}}}{M_{\mathrm{csm,z},\theta}} = 1$

results in:

$\frac{N_{\mathrm{fi,Ed}}}{0.93\times342}+\frac{(1-0.0006N_{\mathrm{fi,Ed}})\times(N_{\mathrm{fi,Ed}}\times0.0094)}{7.76} = 1$

The CSM resistance $N_{\mathrm{fi,Ed}}$ can be determined by solving the previous equation,

$N_{\mathrm{u,csm}} = N_{\mathrm{fi,Ed}} = 238$ kN [the test ultimate load was equal to 280 kN].

7. Conclusions

The fire behaviour and design of hot-rolled steel SHS and RHS under combined compression and bending have been investigated using the finite element analysis. Geometrically and materially nonlinear finite element models were firstly developed and validated using experimental results from a series of cross-sectional tests performed under fire conditions [31]. Upon validation, a systematic parametric study was performed to explore the structural performance of hot-rolled steel SHS and RHS with varying cross-section slendernesses and aspect ratios, subjected to different loading combinations and various elevated temperatures. The results obtained from the parametric study, together with the test data collected from the literature [31], were employed to assess the accuracy of the fire design rules given in EN 1993-1-2 [5] and AISC 360-16 [33]. It was shown that the existing design methods lead to somewhat scattered and often unconservative resistance predictions for SHS and RHS under combined loading at elevated temperatures, owing primarily to the discrete nature of the cross-section classification concept. The continuous strength method (CSM) replaces the traditional cross-section classification concept with a continuous deformation-based design approach, which has been shown to provide more accurate and consistent predictions of cross-section compression and bending resistances at elevated temperatures [41]. The CSM has been extended in the present study to the calculation of the resistance of hot-rolled steel SHS and RHS under combined loading at elevated temperatures; the proposed approach utilises the Eurocode interaction curves but with the CSM compression and bending resistances as the end points. The CSM proposal was shown to yield more consistent resistance predictions than existing methods, with a significantly reduced number of fire predictions lying on the unsafe side. Quantitatively, the COV values of the test and FE to predicted resistance ratios $N_{u,test/FE}/N_{u,csm}$ are 0.058 and 0.100 for cross-sections under compression plus uniaxial and biaxial bending, respectively, which are all significantly lower than those resulting from the current design

codes, and the percentage of the predicted resistances $N_{u,csm}$ lying on the unsafe side is less than 20% of the investigated specimens. Reliability assessment of the proposed CSM was also conducted on the basis of the criteria specified by Kruppa [55], revealing that the CSM provides significantly more reliable resistance predictions for hot-rolled steel SHS and RHS under combined loading at elevated temperatures relative to the existing design methods provided in EN 1993-1-2 [5] and AISC 360-16 [33].

References

[1] X. Yun, L. Gardner, Stress-strain curves for hot-rolled steels, J. Constr. Steel Res. 133 (2017) 36-46.

[2] G.Q. Li, S.C. Jiang, Y.Z. Yin, K. Chen, M.F. Li, Experimental studies on the properties of constructional steel at elevated temperatures, J. Struct. Eng. 129 (2003) 1717-1721.

[3] B.R. Kirby, R.R. Preston, High temperature properties of hot-rolled, structural steels for use in fire engineering design studies, Fire Saf. J. 13 (1) (1988) 27-37.

[4] V. Kodur, M. Dwaikat, R. Fike, High-temperature properties of steel for fire resistance modeling of structures, J. Mater. Civ. Eng. 22 (5) (2010) 423-434.

[5] EC3, Eurocode 3: Design of Steel Structures – Part 1.2: General Rules – Structural Fire Design. BS EN 1993-1-2: 2005, CEN. European Committee for Standardization, Brussels, 2005.

[6] M. Knobloch, J. Pauli, M. Fontana, Influence of the strain-rate on the mechanical properties of mild carbon steel at elevated temperatures, Mater. Des. 49 (2012) 553-565.

[7] K.W. Poh, Stress-strain-temperature relationship for structural steel, J. Mater. Civ. Eng., 13 (5) (2001) 371-379.

[8] A.H. Buchanan, A.K. Abu, Structural design for fire safety, John Wiley & Sons, 2017.

[9] M. Morovat, M. Engelhardt, T. Helwig, E. Taleff, High-temperature creep buckling phenomenon of steel columns subjected to fire. J. Struct Fire Eng., 5 (3) (2014) 189-202.

[10] N.E. Khorasani, P. Gardoni, M. Garlock, Probabilistic fire analysis: material models and evaluation of steel structural members, J. Struct. Eng. 141 (12) (2015) 04015050.

[11] X. Qiang, X. Jiang, F.S. Bijlaard, H. Kolstein, Mechanical properties and design recommendations of very high strength steel S960 in fire, Eng. Struct. 112 (2016) 60-70.

[12] X. Qiang, F.S. Bijlaard, H. Kolstein, Elevated-temperature mechanical properties of high strength structural steel S460N: Experimental study and recommendations for fire-resistance design, Fire Saf. J. 55 (2013) 15-21.

[13] A. Heidarpour, S. Cevro, Q.Y. Song, X.L. Zhao, Behaviour of stub columns utilising mild-steel plates and VHS tubes under fire, J. Constr. Steel Res. 95 (2014) 220-229.

[14] W. Wang, V. Kodur, X. Yang, G.Q. Li, Experimental study on local buckling of axially compressed steel stub columns at elevated temperatures, Thin-Walled Struct. 82 (2014) 33-45.

[15] K.C. Yang, S.J. Chen, C.C. Lin, H.H. Lee, Experimental study on local buckling of fire-resisting steel columns under fire load, J. Constr. Steel Res. 61 (4) (2005) 553-565.

[16] C. Couto, P.V. Real, N. Lopes, B. Zhao, Resistance of steel cross-sections with local buckling at elevated temperatures, J. Constr. Steel Res. 109 (2015) 101-114.

[17] F.A. Ali, D. O'Connor, Structural performance of rotationally restrained steel columns in fire, Fire Saf. J. 36 (7) (2001) 679-691.

[18] K.C. Yang, R. Hsu, Structural behavior of centrally loaded steel columns at elevated temperature, J. Constr. Steel Res. 65 (10-11) (2009) 2062-2068.

[19] D. Winful, K.A. Cashell, S. Afshan, A.M. Barnes, R.J. Pargeter, Behaviour of high strength steel columns under fire conditions, J. Constr. Steel Res. 150 (2018) 392-404.

[20] F.A. Ali, P. Shepherd, M. Randall, I. Simms, D.J. O'Connor, I. Burgess, The effect of axial restraint on the fire resistance of steel columns, J. Constr. Steel Res. 46 (1998) 305-306.

[21] Y.C. Wang, Postbuckling behavior of axially restrained and axially loaded steel columns under fire conditions, J. Struct. Eng. 130 (3) (2004) 371-380.

[22] K.H. Tan, W.S. Toh, Z.F. Huang, G.H. Phng, Structural responses of restrained steel columns at elevated temperatures. Part 1: Experiments, Eng. Struct. 29 (8) (2007) 1641-1652.

[23] Y. Sakumoto, T. Yamaguchi, T. Okada, M. Yoshida, S. Tasaka, H. Saito, Fire resistance of fire-resistant steel columns, J. Struct. Eng. 120 (4) (1994) 1103-1121.

[24] V.K.R. Kodur, M.Z. Naser, Effect of local instability on capacity of steel beams exposed to fire, J. Constr. Steel Res. 111 (2015) 31-42.

[25] M.M.S. Dwaikat, V.K.R. Kodur, A performance based methodology for fire design of restrained steel beams, J. Constr. Steel Res. 67 (3) (2011) 510-524.

[26] J.K. Ahn, C.H. Lee, H.N. Park, Prediction of fire resistance of steel beams with considering structural and thermal parameters, Fire Saf. J. 56 (2013) 65-73.

[27] L. Corradi, C. Poggi, P. Setti, Interaction domains for steel beam-columns in fire conditions, J. Constr. Steel Res. 17 (3) (1990) 217-235.

[28] V.K.R. Kodur, M.M.S. Dwaikat, Response of steel beam-columns exposed to fire, Eng. Struct. 31 (2) (2009) 369-379.

[29] M.M.S. Dwaikat, V.K.R. Kodur, S.E. Quiel, M.E.M. Garlock, Experimental behavior of steel beam-columns subjected to fire-induced thermal gradients, J. Constr. Steel Res. 67 (1) (2011) 30-38.

[30] P.V. Real, N. Lopes, L.S. da Silva, P. Piloto, J.M. Franssen, Numerical modelling of steel beam-columns in case of fire - comparisons with Eurocode 3, Fire Saf. J. 39 (1) (2004) 23-39.

[31] J. Pauli, D. Somaini, M. Knobloch, M. Fontana, Experiments on steel columns under fire conditions, ETH Zurich Institute of Structural Engineering IBK Test Report No. 340, 2012.

[32] M. Knobloch, J. Pauli, D. Somaini, M. Fontana, Stress-strain response and cross-sectional capacity of steel sections in fire, Proc. Inst. Civ. Eng. – Struct. Build. 166 (8) (2013) 444-455.

[33] ANSI/AISC 360-16, Specification for Structural Steel Buildings, AISC, Chicago, 2016.

[34] X. Yun, L. Gardner, N. Boissonnade, Ultimate capacity of I-sections under combined loading–Part 2: Parametric studies and CSM design, J. Constr. Steel Res. 148 (2018) 265-274.

[35] X. Yun, L. Gardner, N. Boissonnade, The continuous strength method for the design of hot-rolled steel cross-sections, Eng. Struct. 157 (2018) 179-191.

[36] L. Gardner, X. Yun, L. Macorini, K. Kucukler, Hot-rolled steel and steel-concrete composite design incorporating strain hardening, Structures 9 (2017) 21-28.

[37] X. Yun, L. Gardner, The continuous strength method for the design of cold-formed steel non-slender tubular cross-sections, Eng. Struct. 175 (2018) 549-564.

[38] X. Yun, L. Gardner, Numerical modelling and design of hot-rolled and cold-formed steel continuous beams with tubular cross-sections, Thin-Walled Struct. 132 (2018) 574-584.

[39] L. Gardner, X. Yun, A. Fieber, L. Macorini, Steel design by advanced analysis: material modeling and strain limits, Engineering 5 (2) (2019) 243-249.

[40] L. Gardner, F. Wang, A. Liew, Influence of strain hardening on the behavior and design of steel structures, Int. J. Struct. Stab. Dy. 11 (05) (2011) 855-875.

[41] M. Theofanous, T. Prospert, M. Knobloch, L. Gardner, The continuous strength method for steel cross-section design at elevated temperatures, Thin-Walled Struct. 98 (2016) 94-102.

[42] ABAQUS Analysis User's Manual, Version 2016. Simulia, Dassault Systèmes, 2016.

[43] X. Yun, L. Gardner, N. Boissonnade, Ultimate capacity of I-sections under combined loading – Part 1: Experiments and FE model validation, J. Constr. Steel Res. 147 (2018) 408-421.

[44] X. Yun, Z.X. Wang, L. Gardner, Structural performance and design of hot-rolled steel tubular cross-sections under combined compression and bending, Eng. Struct. (Submitted).

[45] X. Meng, L. Gardner, A.J. Sadowski, J.M. Rotter. Elasto-plastic behaviour and design of semi-compact circular hollow sections. Thin-Walled Struct. (2020) 106486.

[46] Meng X, Gardner L. Simulation and design of semi-compact elliptical hollow sections. Eng. Struct. 202 (2020): 109807.

[47] T.G. Singh, K.D. Singh, Structural performance of YSt–310 cold–formed tubular steel stub columns, Thin-Walled Struct. 121 (2017) 25-40.

[48] K.T. Ng, L. Gardner, Buckling of stainless steel columns and beams in fire, Eng. Struct. 29 (5) (2007) 717-730.

[49] EC3, Eurocode 3: Design of Steel Structures – Part 1.5: Plated Structural Elements. BS EN 1993-1-5: 2006, CEN. European Committee for Standardization, Brussels, 2006.

[50] EC3, Eurocode 3: Design of Steel Structures – Part 1.1: General Rules and Rules for Buildings. BS EN 1993-1-1: 2005, CEN. European Committee for Standardization, Brussels, 2005.

[51] B.W. Schafer, S. Ádány, Buckling analysis of cold-formed steel members using CUFSM: conventional and constrained finite strip methods, in: Proceedings of the 18th International Specialty Conference on Cold-formed Steel Structures, Orlando, Florida, USA, 2006, pp. 39-54.

[52] L. Gardner, A. Fieber, L. Macorini, Formulae for calculating elastic local buckling stresses of full structural cross-sections, Structures 17 (2019) 2-20.

[53] A. Fieber, L. Gardner, L. Macorini, Design of structural steel members through advanced inelastic analysis with strain limits, Eng. Struct. 199 (2019) 109624.

[54] A. Fieber, L. Gardner, L. Macorini, Structural steel design using advanced inelastic analysis with strain limits, J. Constr. Steel Res. (Submitted).

[55] J. Kruppa, Eurocodes – Fire Parts: Proposal for a methodology to check the accuracy of assessment methods. CEN TC 250, Horizontal Group Fire, Document, 1999, pp. 99-130.

Figures

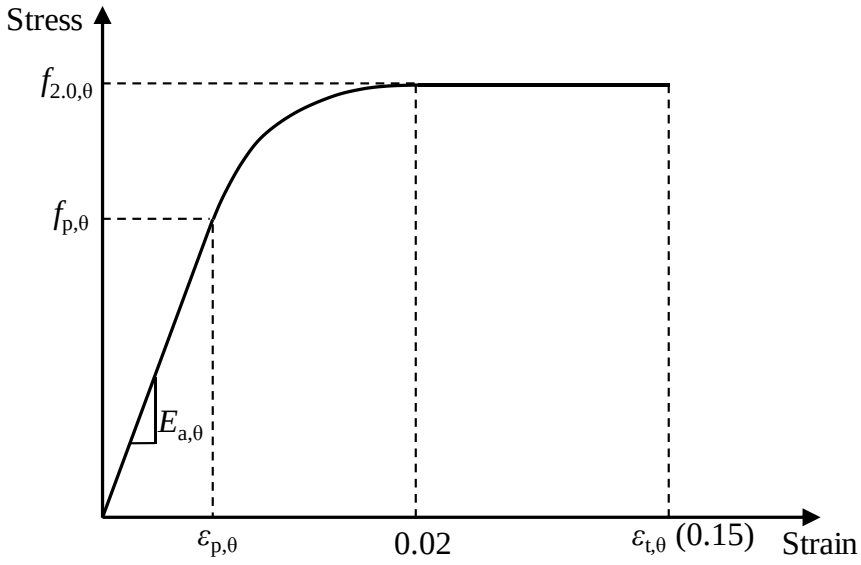

Fig. 1. Stress-strain curve at elevated temperature adopted in EN 1993-1-2 [5]

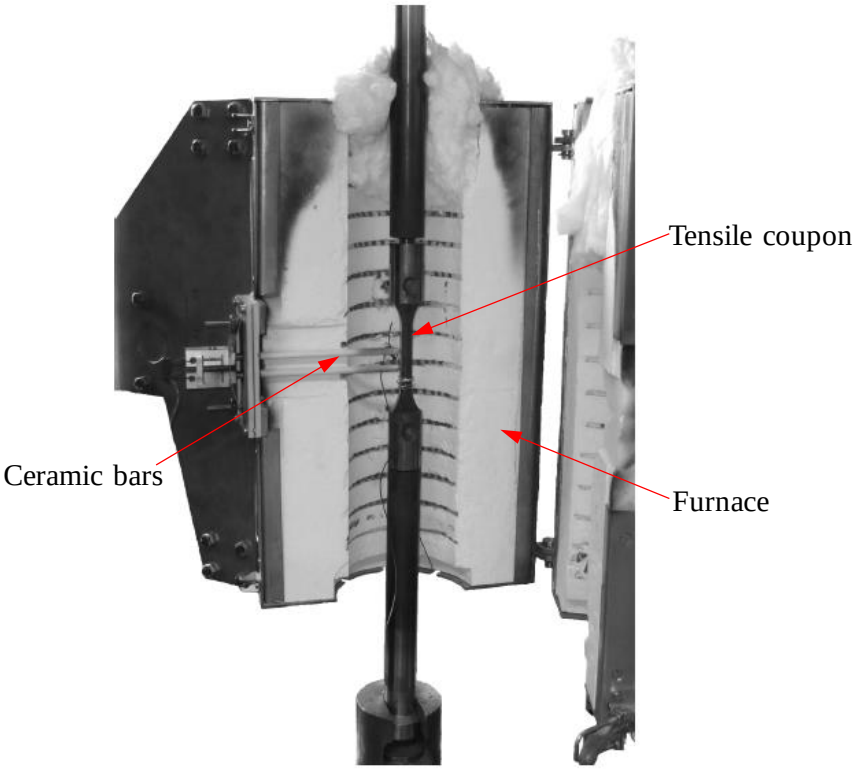

Fig. 2. Test setup for tensile coupon tests at elevated temperatures [31]

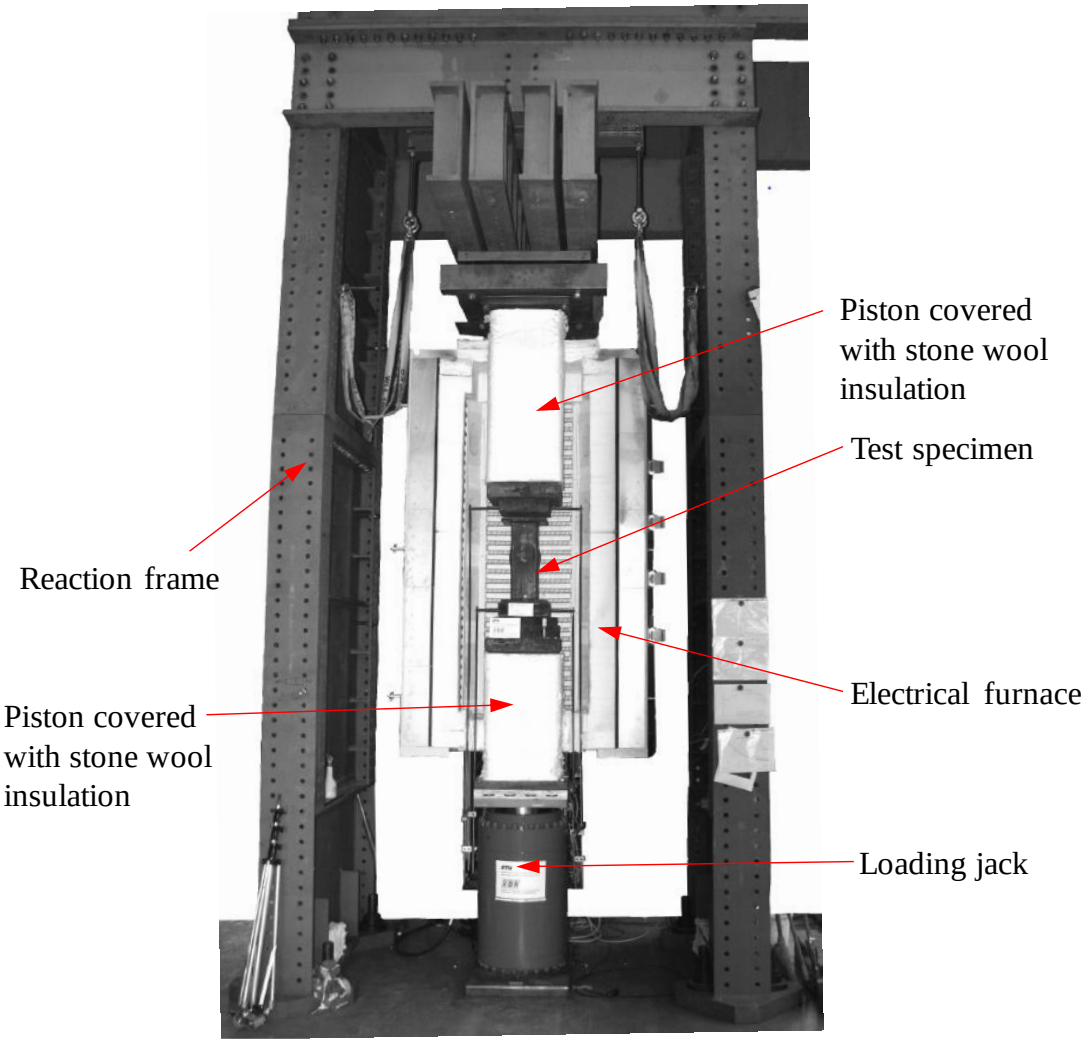

(a) Overview of test setup

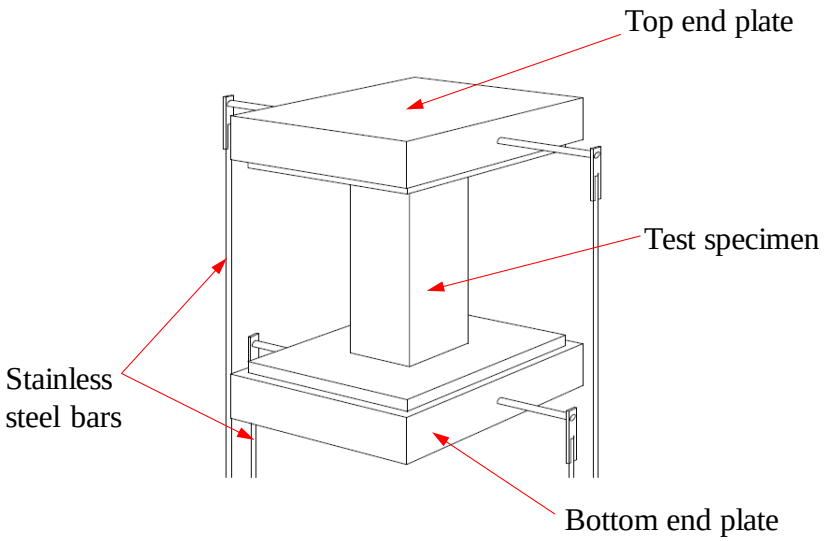

(b) Measurements of relative vertical displacement

Fig. 3. Test setup for stub column tests at elevated temperatures [31]

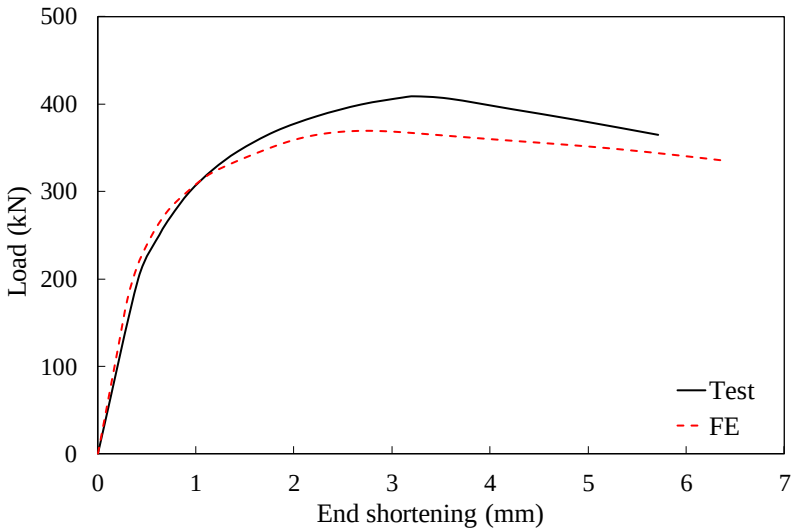

(a)

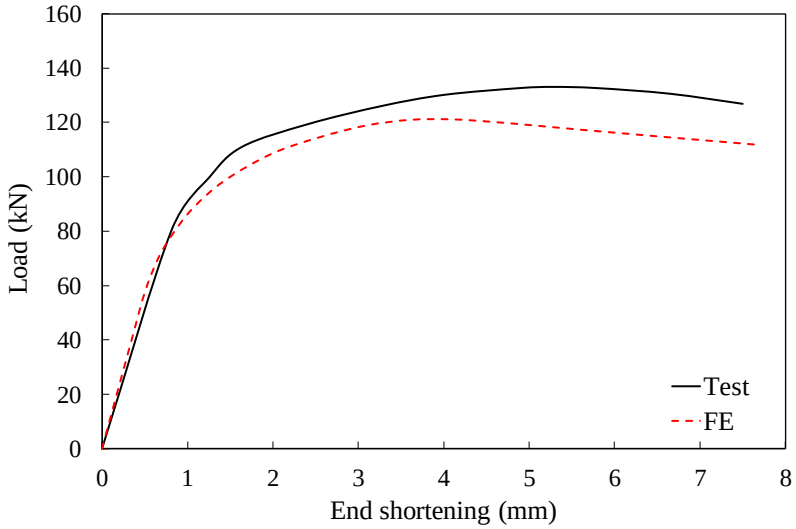

(b)

Fig. 4. Comparison of load-end shortening curves obtained from tests and FE models for specimens (a) RHS120_400C and (b) RHS120_400C_z50

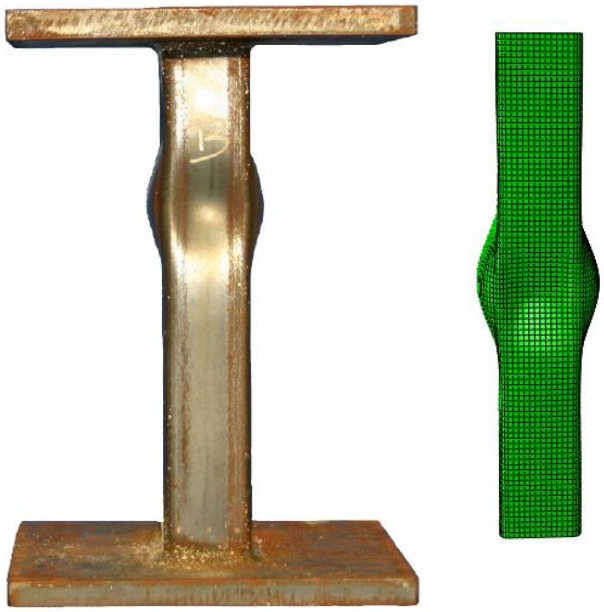

(a)

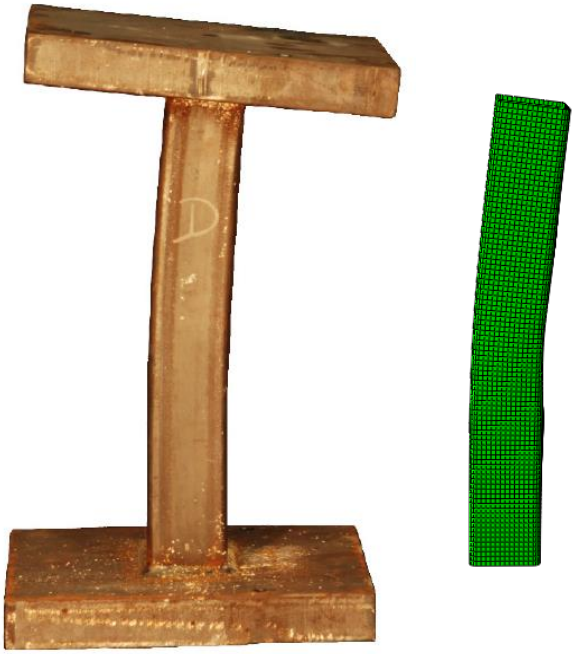

(b)

Fig. 5. Comparison of failure modes obtained from tests and FE models for specimens (a) RHS120_400C and (b) RHS120_400C_z50

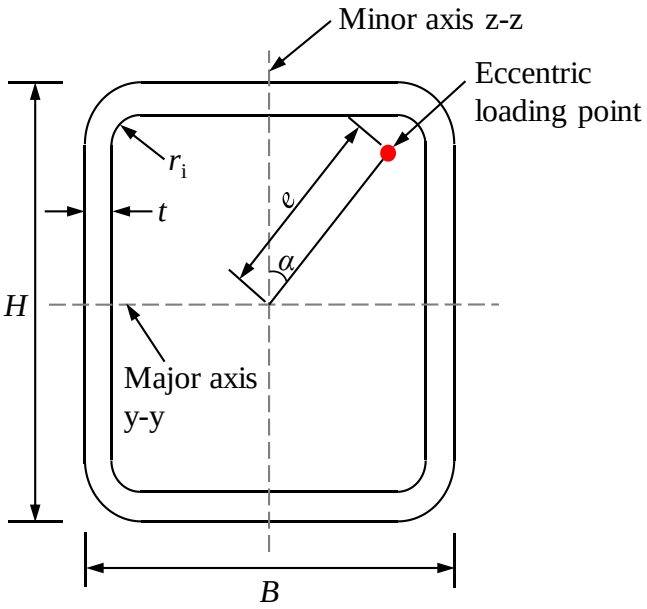

Fig. 6. Definition of loading eccentricity e and loading angle α

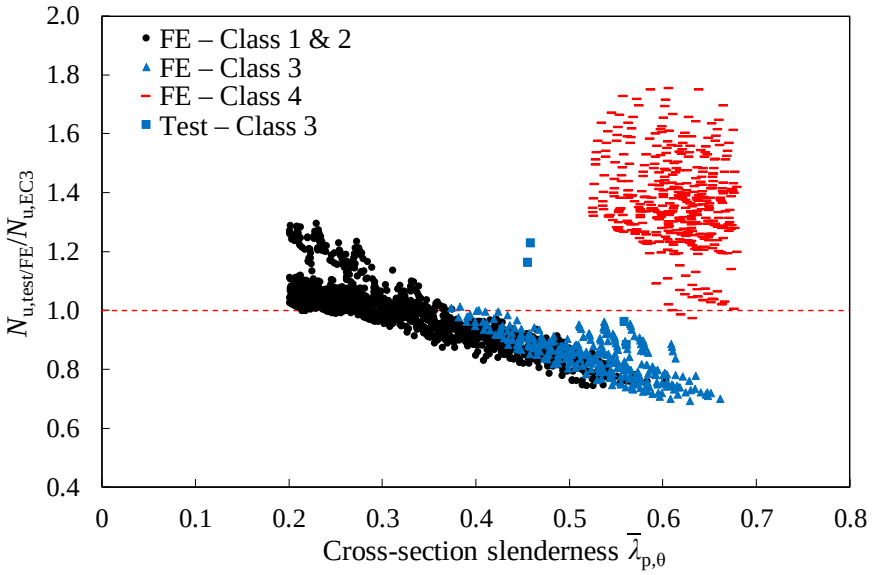

Fig. 7. Comparison of test and FE results with EC3 fire resistance predictions for SHS and RHS under uniaxial bending plus compression

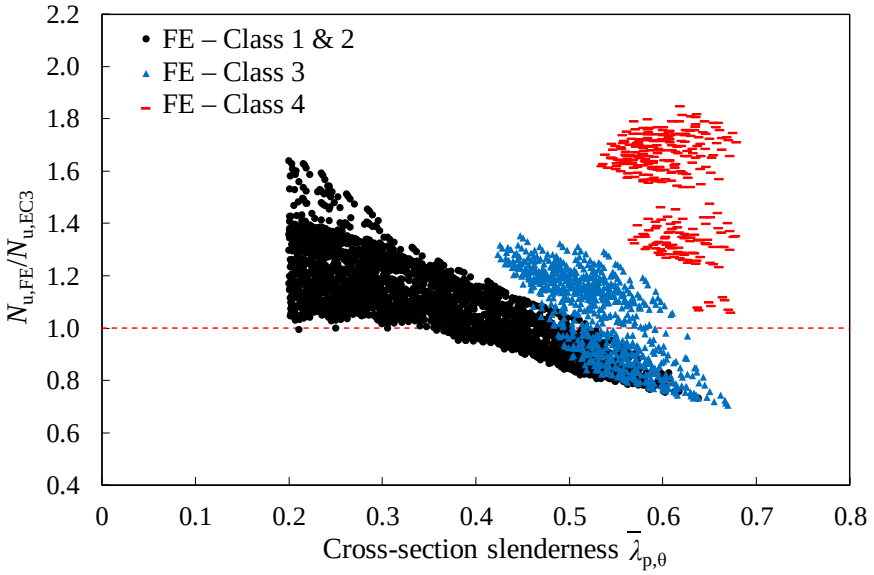

Fig. 8. Comparison of FE results with EC3 fire resistance predictions for SHS and RHS under biaxial bending plus compression

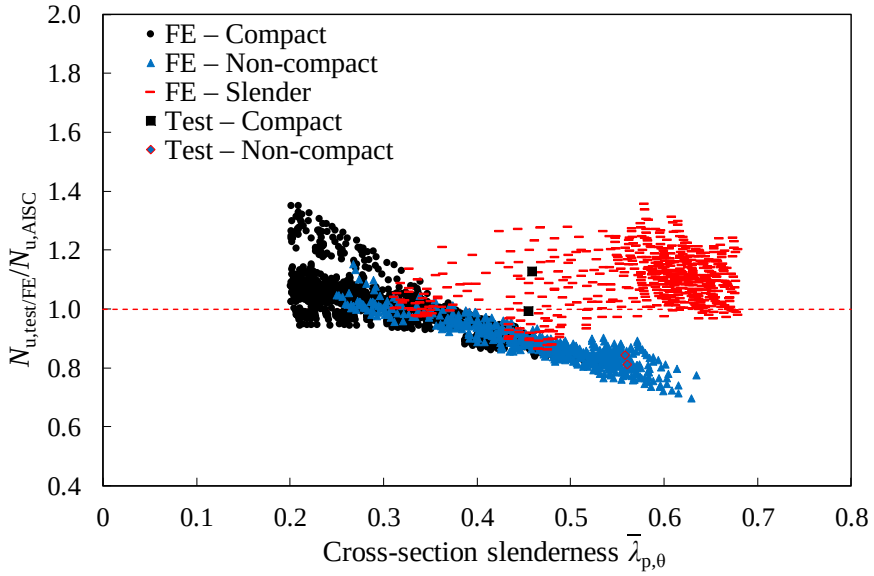

Fig. 9. Comparison of test and FE results with AISC fire resistance predictions for SHS and RHS under uniaxial bending plus compression

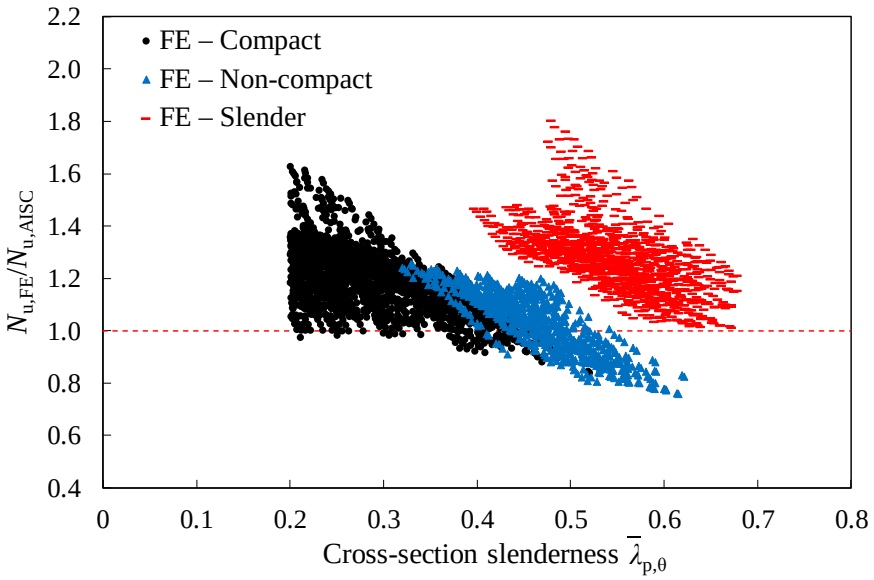

Fig. 10. Comparison of FE results with AISC fire resistance predictions for SHS and RHS under biaxial bending plus compression

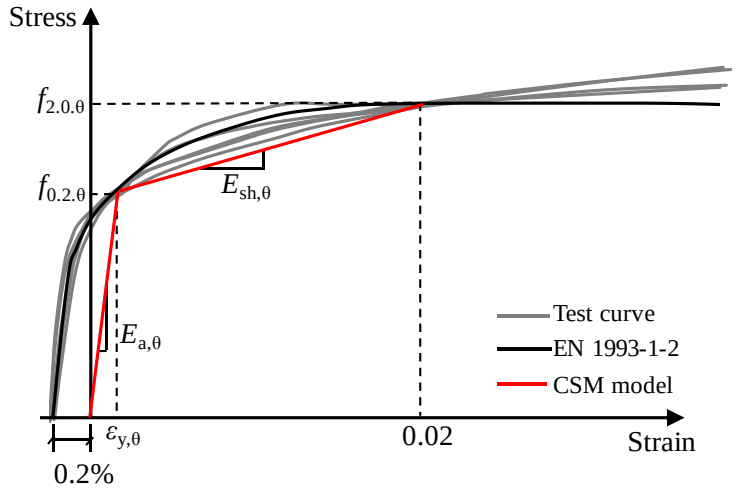

Fig. 11. Adopted bilinear CSM material model and EN 1993-1-2 material model for steel at elevated temperatures; sample experimental stress-strain curves are also shown for comparison purposes

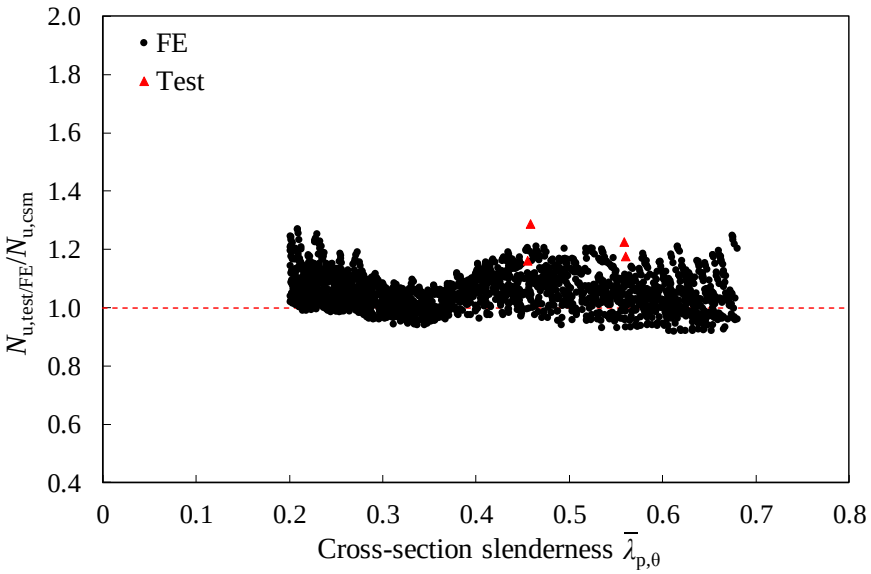

Fig. 12. Comparison of test and FE results with CSM fire resistance predictions for SHS and RHS under uniaxial bending plus compression

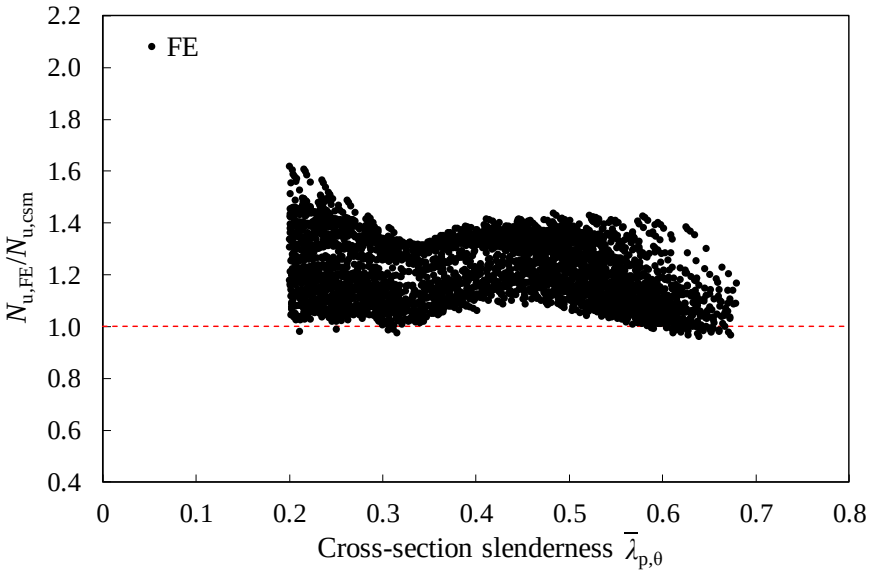

Fig. 13. Comparison of FE results with CSM fire resistance predictions for SHS and RHS under biaxial bending plus compression

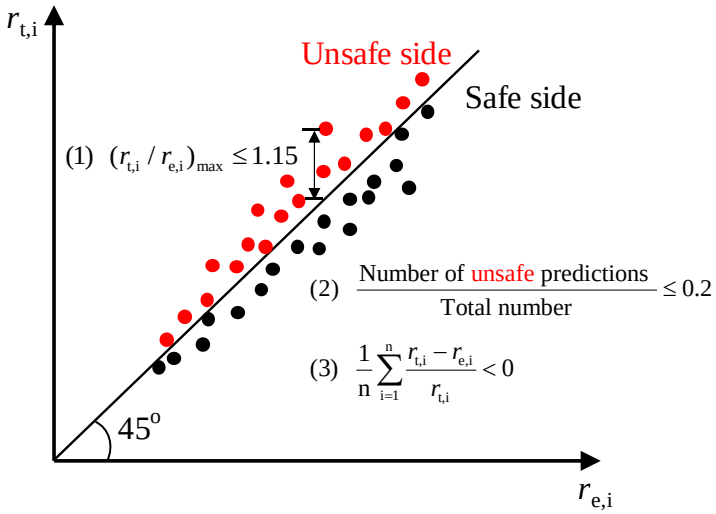

Fig. 14. Schematic illustration of the reliability criteria (1), (2) and (3) specified by Kruppa [55]

Tables

Table 1. Measured dimensions, material properties and test results of hot-rolled steel concentrically and eccentrically loaded stub columns with SHS and RHS [31]

Specimens	Test series	B	H	t	L	e_0	$E_{a,\theta}$	$f_{y,\theta}$	$f_{u,\theta}$	$f_{cr,\theta}$	$N_{u,test}$
		mm	mm	mm	mm	mm	N/mm^2	N/mm^2	N/mm^2	N/mm^2	kN
SHS160_20C	Series 4	160.7	160.3	5.4	479.5	0.7	198700	378	518	885	1225
SHS160_400C		161.5	160.2	5.4	478.8	0.7	162000	324	419	744	795
SHS160_550C		161.6	160.3	5.4	479.3	0.7	102200	157	159	468	468
SHS160_700C		161.2	160.5	5.4	478.8	0.7	39500	41	41	181	138
RHS120_20C	Series 6	60.6	119.3	3.9	356.8	0.4	200700	400	535	1053	483
RHS120_400C		60.5	119.4	3.9	357.5	0.4	160700	352	454	861	408
RHS120_550C		60.6	119.3	3.9	357.3	0.4	104600	188	194	561	257
RHS120_700C		60.5	119.4	3.9	357.5	0.4	57000	55	55	305	74
RHS120_20C_z10		60.6	119.2	3.9	356.5	0.4	200700	400	535	989	356
RHS120_20C_z50		60.6	119.2	3.9	360.0	0.4	200700	400	535	998	161
RHS120_400C_z10		60.5	119.4	3.9	357.8	0.4	160700	352	454	792	280
RHS120_400C_z50		60.5	119.4	3.9	361.8	0.4	160700	352	454	799	133
RHS120_550C_z10		60.6	119.3	3.9	358.0	0.4	104600	188	194	804	205
RHS120_550C_z50		60.5	119.4	3.9	360.3	0.4	104600	188	194	815	87

Table 2. Comparison of test and FE results with different imperfection amplitudes (h/400, h/300, h/200 and measured) for SHS and RHS concentrically and eccentrically loaded hot-rolled steel stub columns at ambient and elevated temperatures

Specimens	$N_{u,test}/N_{u,FE}$			
	h/400	h/300	h/200	Measured
SHS160_20C	1.00	1.01	1.03	1.03
SHS160_400C	0.95	0.97	1.01	1.01
SHS160_550C	0.96	0.97	1.00	1.01
SHS160_700C	0.98	1.00	1.03	1.03
RHS120_20C	0.97	0.97	0.99	1.00
RHS120_400C	1.05	1.08	1.11	1.11
RHS120_550C	1.09	1.11	1.14	1.13
RHS120_700C	1.03	1.04	1.05	1.04
RHS120_20C_z10	1.01	1.02	1.03	1.03
RHS120_20C_z50	0.97	0.98	0.99	0.98
RHS120_400C_z10	1.05	1.07	1.09	1.08
RHS120_400C_z50	1.03	1.05	1.08	1.08
RHS120_550C_z10	1.24	1.25	1.28	1.28
RHS120_550C_z50	1.08	1.10	1.12	1.11
Mean	1.03	1.04	1.07	1.07
COV	0.075	0.074	0.073	0.072

Table 3. Comparison of test and FE results with different predicted fire resistances for SHS and RHS under combined loading

Loading scenarios	Classes		$N_{u,test/FE}/N_{u,EC3}$	$N_{u,test/FE}/N_{u,AISC}$	$N_{u,test/FE}/N_{u,csm}$
Uniaxial bending plus compression No. of tests: 4 No. of FE simulations: 2276	Class 1&2 (Compact)	Mean	0.99	1.02	
		COV	0.097	0.087	
	Class 3 (Non-compact)	Mean	0.85	0.89	
		COV	0.092	0.084	
	Class 4 (Slender)	Mean	1.37	1.10	
		COV	0.107	0.081	
	All	Mean	1.04	1.01	1.06
		COV	0.188	0.114	0.058
Biaxial bending plus compression No. of tests: 0 No. of FE simulations: 3621	Class 1&2 (Compact)	Mean	1.12	1.19	
		COV	0.144	0.107	
	Class 3 (Non-compact)	Mean	1.05	1.03	
		COV	0.154	0.113	
	Class 4 (Slender)	Mean	1.56	1.28	
		COV	0.116	0.099	
	All	Mean	1.14	1.19	1.22
		COV	0.185	0.127	0.100

Table 4. Summary of results from the reliability analyses for different fire design methods

Loading scenarios	Criterion	EN 1993-1-2		AISC 360-16		CSM	
Uniaxial bending plus compression	Criterion 1	15.96%	Fail	13.33%	Fail	0.00%	Pass
	Criterion 2	46.45%	Fail	47.28%	Fail	17.02%	Pass
	Criterion 3	-0.042	Pass	-0.006	Pass	-0.060	Pass
Biaxial bending plus compression	Criterion 1	9.03%	Fail	1.96%	Fail	0.00%	Pass
	Criterion 2	24.80%	Fail	10.19%	Pass	0.88%	Pass
	Criterion 3	-0.142	Pass	-0.191	Pass	-0.221	Pass